Implementation of an antibody characterization process: Application to the major ALS/FTD disease gene C9ORF72

Running title: Antibodies for C9ORF72

Carl Laflamme[1], Paul McKeever[2], Rahul Kumar[1], Julie Schwartz[1], Carol X.-Q. Chen[1], Zhipeng You[1], Shangxi Xiao[2], Faiza Benaliouad[1], Opher Gileadi[3], Heidi M. McBride[1], Thomas M. Durcan[1], Aled Edwards[1,4], Janice Robertson[2] and Peter S. McPherson[1]

[1]Department of Neurology and Neurosurgery, Montreal Neurological Institute, McGill University, Montreal, Quebec, Canada.

[2]Tanz Centre for Research in Neurodegenerative Diseases and Department of Laboratory Medicine and Pathobiology, University of Toronto, Toronto, Ontario, Canada

[3]Structural Genomics Consortium, Nuffield Department of Clinical Medicine, University of Oxford, Oxford, UK

[4]Structural Genomics Consortium, Department of Molecular Genetics, University of Toronto, Toronto, Ontario, Canada

Address correspondence to:
Dr. Peter S. McPherson
Department of Neurology and Neurosurgery
Montreal Neurological Institute
McGill University
3801 University Street
Montreal, QC H3A 2B4
Canada
phone: (514) 398-7355
Email: peter.mcpherson@mcgill.ca

Rigorously characterized antibodies are a key resource in biomedical research, yet there are no community-accepted processes to characterize the quality of research grade antibodies. This has led to a proliferation of poorly characterized antibodies of suspect quality, which in turn has led to flaws in the literature that hamper research progress, including the study of human disease. We selected the human protein C9ORF72 as a test case to implement a more standardized antibody characterization process. Mutations in the gene *C9ORF72* are the major genetic cause of amyotrophic lateral sclerosis and frontotemporal dementia but much remains unknown regarding the function of the encoded protein. We used CRISPR/Cas9-based knockout cells and knockout mice as controls to characterize 14 C9ORF72 antibodies including 12 commercially available antibodies advertised as selective for C9ORF72. We found one monoclonal antibody that is specific for the protein in immunoblot and that also recognizes C9ORF72 specifically in immunohistochemical applications on brain sections. A second C9ORF72 monoclonal antibody is effective for immunoprecipitation and immunofluorescence. Some of the antibodies that do not recognize C9ORF72 have been used in highly cited papers, raising concern over conclusions regarding previously reported C9ORF72 properties.

Introduction

Antibodies are vital tools in the biomedical research arsenal and in keeping with their importance there are over a million unique antibodies that are commercially available. These products include the outputs of several publicly-funded projects that have generated recombinant or monoclonal antibodies, thus creating renewable antibodies with the potential for high reproducibility (Hornsby et al., 2015; Marcon et al., 2015; Na et al., 2016; Venkataraman et al., 2018). The largest antibody initiative has generated greater than 24,000 antibodies corresponding to almost 17,000 human genes, but with a focus on polyclonal antibodies (Uhlen et al., 2015).

The pace and attention given to antibody generation has not been matched with an equal effort on antibody characterization or in implementing standardized antibody characterization procedures. As a result, most products are generated and then sold with only rudimentary and non-quantitative supporting data, and as a result there are serious flaws in the reliability of many of the available reagents. Ill-defined antibodies contribute significantly to a lack of reproducibility in important research efforts including preclinical studies, with estimates that up to 90% of a select group of 53 landmark preclinical studies suffered from such flaws (Bradbury and Plückthun, 2015).

Many of these problems could be alleviated with proper characterization of antibodies, but progress to this end has been impeded by technical, economic and sociological challenges. On the technological front, there are numerous types of antibodies (polyclonal, monoclonal, recombinant) used in many different applications - and each combination will require bespoke characterization. It is time-consuming and for some applications there is no quantitative readout. Second, these characterization processes are expensive and beyond the budget of any single antibody producer. Finally, there is no consensus among often conflicted scientists and companies, many of whom produce the antibodies, as to what the ideal antibody characterization pipeline should comprise. The advent of CRISPR genome-editing technology provides a powerful new approach to aid in antibody validation, and points to the possibility of creating a more standard antibody characterization approach.

Historically, among the primary challenges in developing antibody characterization pipelines was the lack of a suitable control – an isogenic source of proteins lacking the target antigen. This has changed: it is now routine to make knockout (KO) cell lines in an array of cell types,

which, for non-essential proteins, provides the ideal control for testing antibody specificity for the endogenous protein in multiple applications. This capability then opens up the possibility of creating a standard characterization process that can be applied systematically. With such a process in hand, it is possible to begin to characterize many of the existing antibodies, and conceive of a fast, cost-effective way to identify suitable and commercially available antibodies for different applications for the majority of human gene products.

Amyotrophic lateral sclerosis (ALS, OMIM #105400) is a fatal neurodegenerative disease characterized by progressive paralysis leading to respiratory failure and death (Kiernan et al., 2011). ALS is the third most common neurodegenerative disease and there is growing recognition based on clinical, genetic and pathophysiological evidence that it is on a continuum with frontotemporal dementia (FTD, OMIM #600274) (Ng et al., 2015). A search for genes involved in ALS-FTD led to the discovery of a hexanucleotide-repeat expansion mutation in the first intron of *C9ORF72*. Analysis of an extended clinical series from North America revealed that this mutation underlies 11.7% and 23.5% of familial FTD and ALS cases, respectively, and in a large Finnish population, the *C9ORF72* mutation was found to underlie 46.0% of familial ALS and 21.1% of sporadic ALS (DeJesus-Hernandez et al., 2011; Renton et al., 2011). Thus, the *C9ORF72* mutation is the most common genetic abnormality in both FTD and ALS. Although there is debate as to how the non-coding mutation in *C9ORF72* leads to disease it appears likely that loss-of-function mechanisms resulting from haploinsufficiency contribute to disease pathophysiology (DeJesus-Hernandez et al., 2011; Renton et al., 2011; Shi et al., 2018). Even if the mutation causes the disease through a predominant toxic gain-of-function mechanism therapeutic strategies aimed at reducing expression of the mutant allele will lead to decreased expression of the protein. Thus, it is vital to understand the cell biological role of C9ORF72.

In order to understand the function of C9ORF72, many antibodies have been developed and are commercially available. Here, we implemented a validation procedure, outlined in the discussion, to identify high quality antibodies from among them. We identified a monoclonal antibody that is effective and specific for immunoblot and immunohistochemical applications and another that that is effective for immunoprecipitation and immunofluorescence applications.

Results

Specificity testing of C9ORF72 antibodies by immunoblot

We began by purchasing known commercial antibodies for C9ORF72. For this we searched the literature by PubMed and examined the websites of companies with C9ORF72 antibodies identified using Google searches. We avoided purchasing the same antibody available from different companies. For example, the C9ORF72 antibody *Prestige Antibodies® Powered by Atlas Antibodies* was purchased at Sigma (HPA023873), but is also sold by other companies including Novus Biological (NBP1-93504). We identified 12 commercial C9ORF72 antibodies, 9 rabbit polyclonal antibodies and 3 mouse monoclonal antibodies (Table 1). The antibodies are available from Abcam (4), Proteintech (3), GeneTex (3), Sigma (1), and Santa Cruz (1). In addition we identified 2 sheep polyclonal antibodies from the Protein Phosphorylation and Ubiquitylation Unit of the Medical Research Council (MRC) in Dundee Scotland (Table 1).

Initially we screened the 14 C9ORF72 antibodies by immunoblot using lysates of HEK-293 cells including parental cells, an isogenic heterozygous line in which C9ORF72 was deleted from a single allele, and two isogenic lines in which C9ORF72 was depleted from both alleles (Fig. 1). The heterozygous and KO status of the lines was confirmed by genomic sequencing. We chose HEK-293 cells because they are easy to edit using CRISPR and after confirming that C9ORF72 is expressed in these cells by referencing PaxDb, a protein abundance database based on proteomic analysis of multiple tissues and cell types in numerous species (Wang et al., 2015) (https://pax-db.org/). The relatively high abundance of C9ORF72 in HEK-293 was subsequently confirmed by immunoblot (Fig. 4).

For each series of blots, we prepared lysates from the HEK-293 cell lines and resolved 50 μg of protein from each on 5-16% gradients gels. Lysates were prepared in buffer containing 1% Triton X-100 in order to extract both cytosolic and membrane-associated proteins. The proteins transferred to nitrocellulose membranes were stained with Ponceau to ensure even loading of lysates. After screens of all 14 antibodies we found one mouse monoclonal antibody from GeneTex (GTX634482) that has optimal features. It shows a strong signal in parental HEK-293 cell lysates, the signal is reduced by ~50% in the heterozygous line, and no signal for the antibody is detected in the two KO lines. Moreover, there are no other bands visible (Fig. 1), even upon long exposure (Fig. S1). Thus, the signal to noise ratio in HEK-293 cells is sufficient

to justify their use in immunoblot screens. GeneTex monoclonal GTX632041 also recognizes C9ORF72 seemingly selectively in the short exposure (Fig. 1) but other bands are detected following longer exposure (Fig. S1). Other antibodies that recognize C9ORF72 include ab12179 from Abcam, PT25757 and PT22637 from Proteintech, HPA023873 from Sigma and MRC-S478D and MRC-S479D from the MRC. However, all these antibodies detect additional bands, and in several cases they have multiple cross-reactivity. Six of the antibodies do not detect endogenous C9ORF72. Thus, GTX634482 from GenTex is a robust antibody for immunoblot (Fig. 1/4).

Testing C9ORF72 antibodies by immunoprecipitation

We next sought to test the functionality of the antibodies in immunoprecipitation applications. Each of the 14 antibodies was pre-coupled to protein A or protein G Sepharose as appropriate and a detergent solubilized HEK-293 cell lysate was prepared and incubated with the antibody/bead mixtures. For controls we incubated the HEK-293 lysates with beads alone or the bead/antibody conjugates were incubated with buffer alone. After washing the beads, the presence of C9ORF72 in the immunoprecipitates was detected by blot using rabbit antibody PT22637 for the immunoprecipitates with mouse antibodies and the mouse antibody GTX634482 for immunoprecipitates with rabbit or sheep antibodies (Fig. 2). Of the 14 antibodies tested, 9 are able to immunoprecipitate endogenous C9ORF72 with GeneTex monoclonal antibody GTX632041 demonstrating the most robust enrichment of the protein compared to starting material (Fig. 2). Five antibodies showed no appreciable C9ORF72 immunoprecipitation including GTX634482 (Fig. 2), which was the most effective antibody in immunoblot.

Using mass spectrometry we then assessed the degree to which GTX632041 was selective for C9ORF72 and able to co-purify SMCR8, a known obligate interacting partner of the protein (Sellier et al., 2016; Amick et al., 2016; Zhang et al., 2018). We performed immunoprecipitation studies with GTX632041 using parental and KO HEK-293 cell lysates. When we examined the soluble cell lysate (starting material, SM) and the unbound proteins (UB) of immunoprecipitations from the parental cells we observe that a significant proportion of C9ORF72 and SMCR8 are removed from the lysate by immunoprecipitation with antibody GTX632041 and that both proteins are strongly enriched in the immunoprecipitated sample relative to SM (Fig. 3). None of the other 13 antibodies allow for an appreciable co-immunorpecipitation of SMCR8 (data not shown). Mass spectrometry of the samples

immunoprecipitated with GTX632041 reveals C9ORF72 (13 peptides), SMCR8 (51 peptides), and another known C9ORF72-binding partner WDR41 (23 peptides) (Sellier et al., 2016) (Fig. 3). The presence of C9ORF72 and its known-binding partners at near 1:1:1 levels (when adjusting for the mass of the proteins) further supports the use of HEK-293 cells in our analysis. No peptides are detected for any of these proteins by mass spectrometry of immunoprecipitates performed under identical conditions (including the presence of the GTX632041 antibody) from lysates of C9ORF72 KO cells, further demonstrating the specificity of the antibody for C9ORF72.

Specificity testing of C9ORF72 antibodies by immunofluorescence

We next tested the effectiveness of the antibodies for immunofluorescence applications. HEK-293 cells, parental and KO were fixed in paraformaldehyde (PFA) and stained with C9ORF72 antibodies with appropriate fluorescent secondary antibodies. The antibodies give various staining patterns primarily composed of a distributed punctate pattern but a very similar pattern is seen in the KO cells with no reduction in fluorescent staining (Fig. S2). In fact none of the 14 antibodies tested give a staining pattern that is discernibly altered in KO cells. Similar results were seen when the cells are fixed in -20°C methanol (Fig. S3).

Achieving successful detection of endogenous proteins by immunofluorescence can be challenging, especially for lower abundance proteins. In an effort to obtain a better signal to noise ratio, we sought to identify a cell line with higher levels of endogenous C9ORF72 expression. We thus used GTX634482, validated as described (Fig. 1) to determine the relative levels of C9ORF72 in multiple tissues and cell lines employing the LI-COR Odyssey Imaging System (LI-COR Biosciences), which utilizes fluorescent secondary antibodies to allow for quantitative immunoblots. The mouse ortholog of C9ORF72 is 98% identical to the human protein and we confirmed the utility of the anti-human GTX634482 in immunoblots of extracts from mouse tissues. C9ORF72 is detected at the highest levels in mouse brain with lower levels in spinal cord and testis (Fig. 4A). Less C9ORF72 protein is detected in a series of non-neuronal tissues including immune tissues and no signal is observed in brains of C9ORF72 KO mice (Fig. 4A). C9ORF72 is also detected in a variety of cell lines including human U2OS (osteocarcoma), human HEK-293, mouse RAW264.7 cells (macrophages), MEFs (mouse embryonic fibroblasts), rat PC12 (pheochromocytoma), human HeLa, human RKO (colon carcinoma), and human U87 and U251 (glioblastomas) (Fig. 4A/B). C9ORF72 is detected in

human motor neuron precursor cells (NPCs) and motor neurons (MNs) derived from human-induced pluripotent stem cells (Fig. 4B) at levels similar to HEK-293.

Of the cells lines tested, U2OS has near the highest levels of C9ORF72 (approximately 1.5 times that of HEK-293 cells) (Fig. 4B), are easy to genome edit and are large cells suitable for immunofluorescence analysis. We thus sought to test the C9ORF72 antibodies in U2OS cells. We first used CRISPR/Cas9 to generate U2OS cells lacking C9ORF72, which was confirmed by genomic sequencing (data not shown) and immunoblot with GTX634482 (Fig. 5A). As a control we used gRNAs that target the adeno-associated virus (AAV) AAVS1 locus in the U2OS cells. To better distinguish between the parental and C9ORF72 KO lines, we transfected LAMP1-YFP in AAVS1-targeted control cells and LAMP1-RFP in C9ORF72 KO cells. We then re-plated the cells such that both control and KO cells were found on the same coverslip as a mosaic (Fig. 5B). This strategy reduces microscopy imaging and figure processing biases. We chose LAMP1 since a tagged form of C9ORF72 was shown to distribute to LAMP1-positive lysosomes (Amic et al., 2016). Using this strategy we find GTX632041 as the sole antibody able to recognize endogenous C9ORF72 specifically. Indeed, GTX632041 immunofluorescence labeling reveals a cytosolic/punctate fluorescence signal that is dramatically reduced in KO cells to a level comparable to buffer control (Fig. 5C). The other 13 antibodies show non-specific staining patterns that are similar between control and KO cells (Fig. 5C and Fig. S4).

Identification of C9ORF72 antibodies effective for immunohistochemistry

Given the importance of C9ORF72 in ALS and FTD it is vital to identify an antibody that is effective for staining of tissue sections. We thus used diaminobenzidine (DAB) labeling comparing brain sections from wild-type littermate mice to mice with the C9ORF72 ortholog (31100432021Rik) deleted (Jiang et al., 2016). We originally focused on using GTX634482, which is the strongest and most specific antibody for immunoblot on HEK-293 cells (Fig. 1), and also recognizes the protein in mouse brain (Fig. 4A), on sections that had been treated for epitope unmasking. A punctate and/or neuritic-like signal is observed in the neuropil of the glomerular layer of the olfactory bulb, the ventral pallidum of the basal ganglia, the CA4 (hilus), CA3, and CA2 region of the hippocampus, the substantia nigra, the inferior olive, and granular layer of the cerebellar cortex of wild-type mice (Fig. 6A, arrows). The signal is nearly completely ablated in the KO mice although there is some non-specific signal seen in the dentate gyrus/CA4, inferior olive and cerebellar cortex sections (Fig. 6A, arrowheads). The staining pattern observed is similar to the basal ganglia, hippocampal formation, and cerebellum staining

observed in a previous study (Frick et al., 2018). GTX632041, which is the most effective antibody for immunoprecipitation (Fig. 2/3) and immunofluorescence (Fig. 5) analysis, also specifically recognizes C9ORF72 in mouse brain sections including those through the hippocampus (Fig. 6B) but staining is not as strong or consistently specific as seen with GTX634482.

In conclusion, we have identified antibodies that effectively and specifically recognize C9ORF72 in multiple applications. Mouse monoclonal antibody **GTX634482** is recommended for immunoblot and immunohistochemical applications on antigen unmasked samples, and **GTX632041** is recommended for immunoprecipitation and immunofluorescence.

Discussion

Many *ad hoc* international working groups have met to help define best practices for antibody validation (Taussig et al., 2018). One of the groups (Uhlén et al., 2016) proposed 5 separate validation criteria: 1) genetic strategies in which the specificity of the antibody toward the endogenous protein is confirmed by the loss of signal in cells or tissues comparing parental to KO or knockdown controls (if the gene is essential); 2) orthogonal strategies in which correlations are made between the antibody signal and known information regarding protein abundance or localization; 3) the ability of two independent uncharacterized antibodies recognizing different epitopes in the same target protein to recognize the same protein; 4) using epitope-tagged proteins comparing blots with antibodies against the tag to blots with the uncharacterized antibody; 5) immunoprecipitation followed by mass spectrometry to determine if the protein of interest is a major signal in the sample. These criteria are arguably not of equal scientific value. The first and fifth methods are the most unbiased and useful, particularly if combined. The remaining ones are less informative. Criterion 5 provides unequivocal information about the ability of the antibody to detect the endogenous protein in immunoprecipitation applications. However, it cannot distinguish those proteins recognized by the antibody from those that are non-specifically bound. Moreover, it does not give insight into the utility of the antibody for other applications. The genetic approaches presented in criterion 1 are suitable for antibody validation in all applications.

Mutations in C9ORF72 are the major known cause of heritable forms of ALS and FTD (DeJesus-Hernandez et al., 2011; Renton et al., 2011) and it is thus important to understand the basic cell biology of the protein. Of the between 0.5 and 3 million antibodies held by biological supply companies, we found 12 C9ORF72 antibodies (plus two more from the MRC, an academic institution). The antibodies were tested for effectiveness in 4 separate commonly used approaches, immunoblot, immunoprecipitation, immunofluorescence on cells and immunohistochemistry on tissue sections, comparing signals found in parental/wild-type samples to KO controls. We identified only one antibody (monoclonal GTX634482 from GeneTex) that is uniquely specific for C9ORF72 in immunoblots. This antibody is also effective and specific for use in immunohistochemistry on sections from mouse brain that have been treated with high temperature and acid to unmask epitopes hidden by protein conformation. Thus, this antibody appears to recognize an epitope that is exposed predominantly in denatured C9ORF72. Another monoclonal antibody was identified (monoclonal GTX632041 from

GeneTex) that effectively immunoprecipitates C9ORF72 and detects endogenous C9ORF72 by immunofluorescence. This antibody therefore appears to recognize the native form of the protein.

Here we set out to develop and implement an antibody characterization process to identify appropriate antibodies for any selected protein using the major ALS/FTD disease gene C9ORF72 as a test case. We originally queried PaxDb, a comprehensive protein abundance database that compares protein levels across tissues and cell lines using a standardized spectral counting pipeline (Wang et al., 2015), to identify a cell line that expresses C9ORF72 and has good characteristics for genome editing and screening. PaxDb reports that while overall C9ORF72 is a low abundance protein, its expression in HEK-293 cells is comparable to or moderately higher than most other cell lines. We thus generated C9ORF72 KO lines in HEK-293 cells that we screened by immunoblot, immunoprecipitation and immunofluorescence. While the signal to noise ratio was satisfactory for immunoblot and immunoprecipitation, we discovered that it was not suitable for immunofluorescence. We thus screened additional cell lines and tissues by quantitative immunoblot using the immunoblot validated antibody. This led us to re-screen all C9ORF72 antibodies by immunofluorescence in control versus C9ORF72 KO U2OS cells, which revealed an antibody suitable for immunofluorescence. Based on this study we propose a validation workflow as follows: 1) identify all commercial antibodies against a protein of interest; 2) use PaxDB to identify cell lines that express the protein of interest at relatively high levels and are readily modifiable by CRISPR/Cas9; 3) generate a KO cell line and screen the antibodies by quantitative immunoblot; 4) Use specific antibodies determined from step 3 to screen panels of cell lines; 5) based on the information in step 4 choose a cell line that has high expression of the protein of interest, is amenable to editing by CRISPR/Cas9, and has appropriate characteristics for the target of interest; 6) use the selected edited line to screen antibodies for specificity by immunoprecipitation and immunofluorescence; 7) select specific antibodies for use in more intensive processes such as immunohistochemistry. While this is a pipeline that is applicable to identifying appropriate antibodies from antibody panels, the principles can be applied to any selected antibody for any individual application.

The two GeneTex mouse monoclonal antibodies effective for immunoblot, immunoprecipitation, immunohistochemistry and immunofluorescence have not yet been used in a published paper, whereas the GeneTex rabbit polyclonal antibody (GTX119776), which does not detect the protein by blot and only weakly immunoprecipitates has been used in 5 published papers (Table

1). A troubling finding of our study is that the rabbit polyclonal antibody SC-138763, which clearly does not recognize C9ORF72 in any application, has been used in 15 published manuscripts to ascribe specific properties to the protein in normal and disease states (Table 1). A Google Scholar-based bibliometric approach revealed that those 15 papers have been cited greater than 3000 times and that first layer citations to those citing papers equals greater than 66000 citations. While clearly the majority of first and second layer citations do not focus on discoveries related to the use of the antibody in the original 15 papers, this simple analysis reveals the cumulative and sustained impact of inadequate characterization of antibodies.
These studies were supported by the Motor Neurone Disease Association (UK), The ALS Association (USA) and ALS Canada. We will now use the developed criteria to provide validation testing on antibodies raised against a prioritized list of gene products that are altered in genetic forms of ALS.

Material and Methods

Antibodies

All C9ORF72 antibodies are listed in Table 1. SMCR8 antibody is from Abcam (ab202283). WDR41 antibody is from Abgent (AP10866B-EV). Peroxidase-conjugated goat anti-mouse and anti-rabbit are from Jackson ImmunoResearch Laboratories. Odyssey IRDye 800CW goat anti-mouse-HRP, the REVERT total protein stain solution and the Odyssey Blocking buffer (TBS) are from LI-COR Biosciences. Alexa Fluor 647-conjugated mouse and rabbit secondary antibodies are from Invitrogen.

Mouse breeding

Mice were bred and cared for in accordance with the guidelines of the Canadian Council on Animal Care following protocols approved by the University of Toronto Animal Care Committee. C9ORF72 KO mice were a generous gift from Dr. Don Cleveland (UCSD) and Dr. Clothilde Lagier-Tourenne (UMass). In-house breeding and genotyping were performed as previously described (Jiang et al., 2016). Briefly, heterozygous C9ORF72 mice (C57BL/6 background) were crossed to produce homozygous C9ORF72 KO mice, heterozygous C9ORF72 mice, and wild-type littermates. For all experiments, approximately 3-month old C9ORF72 KO and wild-type littermates were used, which was an empirically selected time point. Mouse tissues were prepared for immunohistochemistry or immunoblot as described in separate sections below.

Cell culture

HEK-293 were cultured in DMEM high-glucose (GE Healthcare cat# SH30081.01) containing 10% bovine calf serum (GE Healthcare cat# SH30072.03), 2 mM L-glutamate (Wisent cat# 609065, 100 IU penicillin and 100µg/ml streptomycin (Wisent cat# 450201). U2OS were cultured in DMEM high-glucose containing 10% tetracyclin-free fetal bovine serum (FBS) (Wisent cat# 081150) 2 mM L-glutamate, 100 IU penicillin and 100 g/ml streptomycin. Tetracyclin-free FBS was used to limit Cas9 expression.

CRISPR/Cas9 genome editing

For the KO HEK-293 cells, a C9ORF72 KO gRNA was annealed and ligated into Bbs1-digested pSpCas9(BB)-2A-Puro (PX459) V2.0 vector. PX459 V2.0 was a gift from Feng Zhang (Addgene plasmid # 62988). The gRNA was designed using the “optimized CRISPR design” tool

(www.crisp.mit.edu). Oligonucleotides with Bsb1 cleavage overhangs were annealed and cloned into the Cas9/puromycin expressing vector (PX459 from Addgene #48139). The following gRNA sequence was used to create the KO line: CAACAGCTGGAGATGGCGGT. Genome editing plasmids expressing gRNA were transfected in HEK-293 cells using jetPRIME Transfection Reagent (Polyplus) according to the manufacturer's protocol. The next day, transfected cells were selected using 2 µg/ml puromycin for 24 h. At 96 h post-selection, cells were isolated by clonal dilution. Following the selection expansion of colonies, KOs were confirmed by sequencing of PCR-amplified genomic DNA (data not shown) and immunoblot. Genomic DNA was extracted using QuickExtract DNA extraction solution (Epicentre Biotechnologies).

For the KO U2OS cells, we first generated a line with stable-inducible Cas9. The line was generated using the pAAVS1-PDi-CRISPRn knockin vector and the TALEN pair arms were gifts from Bruce Conklin (Addgene plasmid # 73500) (Mandegar et al., 2016). U2OS cells were resuspended in complete media and $1X10^5$ cells were mixed with pAAVS1-PDi-CRISPRn knockin vector (0.25 ug) and each AAVS1 TALEN pair (0.1 ug) and nucleofected using the Neon® Transfection System (program 17; Life Technologies). Polyclonal population was selected with 2 µg/ml of puromycin (Bioshop cat# PUR555). Seventy-two hours post-treatment, single cells were plated in a 96-well plate. U2OS-PDi-CRISPRn positive clones were detected by PCR and the presence of the PDi-CRISPRn knockin platform into the safe-harbor AAVS1 locus was confirmed by Sanger sequencing.

To generate the C9ORF72 KO, synthetic single gRNAs (sgRNAs) were designed using the CRISPR Design Tool from Synthego (https://www.synthego.com/products/bioinformatics/crispr-design-tool). The sgRNAs (from Synthego) were transfected in the stable-inducible Cas9 U2OS cell line using JetPRIME transfection reagent. At 1 hr post transfection, Cas9 expression was induced by treating cells with 2 µg/ml of doxycycline (Bioshop cat# DOX44). The next day, media was changed to remove doxycycline and stop the expression of Cas9. C9ORF72 KO cells were isolated by clonal dilution and KOs were confirmed by sequencing of PCR-amplified genomic DNA and immunoblot. Genomic DNA was extracted using QuickExtract DNA extraction solution (Epicentre Biotechnologies). C9ORF72 targeting sgRNA1: GCAACAGCUGGAGAUGGCGG, C9ORF72 targeting sgRNA2: GUCUUGGCAACAGCUGGAGA, AAVS1 locus targeting sgRNA1.2:

GGGGCCACUAGGGACAGGAU and AAVS1 locus targeting sgRNA 1.3: GUCCCCUCCACCCCACAGUG

Immunoblot

Cultured cells were collected in HEPES lysis buffer (20 mM HEPES, 100 mM sodium chloride, 1 mM EDTA, 5% glycerol, 1% Triton X-100, pH 7.4) supplemented with protease inhibitors. Following 30 min on ice, lysates were spun at 238,700xg for 15 min at 4°C and equal protein aliquots of the supernatants were analyzed by SDS/PAGE and immunoblot. Mouse tissues were homogenized in HEPES lysis buffer (without detergent) using a glass/Teflon homogenizer with 10 strokes at 2000 rpm and Triton X-100 was added to 1% final concentration. Following 30 min on ice, mouse tissues lysates were spun at 238,700xg for 15 min at 4°C. Equal protein aliquots of the supernatants were analyzed by SDS/PAGE and immunoblot. Immune cell populations were prepared from spleen, thymus and bone marrow by disrupting the tissue in media using a sterile syringe plunger as a pestle and passing the slurry through a 40 µm cell strainer. Red blood cells from were removed using a red blood cell lysis buffer (155 mM NH_4Cl, 12 mM $NaHCO_3$, 0.1 mM EDTA). Equal protein aliquots of the supernatants were analyzed by SDS/PAGE and immunoblot.

Immunoblots were performed with large 5-16% gradient polyacrylamide gels and nitrocellulose membranes. Proteins on the blots were visualized by Ponceau staining. Blots were blocked with 5% milk, and antibodies were incubated O/N at 4°C with 5% bovine serum albumin in TBS with 0.1% Tween 20 (TBST). The peroxidase conjugated secondary antibody was incubated in a 1:10000 dilution in TBST with 5% milk for 1 h at room temperature followed by washes. For quantitative immunoblot in figure 2, nitrocellulose transfers were incubated with REVERT total protein stain to quantify the amount of protein per lane, than blocked in Odyssey Blocking buffer (TBS) and C9ORF72 antibody GTX634482 was incubated O/N at 4°C in TBS, 5% BSA and 0.2% Tween-20. The secondary antibody (Odyssey IRDye 800CW) was incubated in a 1:20000 dilution in TBST with 5% BSA for 1 h at room temperature followed by washes. Detection of immuno-reactive bands was performed by image scan using a LI-COR Odyssey Imaging System (LI-COR Biosciences) and data analysis was done using LI-COR Image Studio Lite Version 5.2.

Immunoprecipitation

HEK-293 cells were collected in HEPES lysis buffer supplemented with protease inhibitors. Following 30 min on ice, lysates were spun at 238,700xg for 15 min at 4°C. One ml aliquots at 1 mg/ml of lysate were incubated for ~18 h at 4°C with either 1 µg of a C9ORF72 antibody coupled to protein A or G Sepharose. Beads were subsequently washed four times with 1 ml of HEPES lysis buffer, and processed for SDS-PAGE and immunoblot. For immunoprecipitation with GTX632041 prior to mass spectrometry, HEK-293 cells (parental and C9ORF72 KO) were collected in HEPES lysis buffer supplemented with protease inhibitors. Following 30 min on ice, lysates were spun at 238,700xg for 15 min at 4°C. One ml aliquots at 1 mg/ml were incubated with empty protein G Sepharose beads for 30 min to reduce the levels of proteins bound non-specifically. These pre-cleared supernatants were incubated for 4 h at 4°C with GTX632041 antibody coupled to protein G Sepharose. Following centrifugation, the unbound fractions were collected and the beads were washed 3 times with 1 ml of HEPES lysisi buffer. The beads were then suspended in 1X SDS gel sample buffer. Fractions of the sample were processed for immunoblot. Parallel fractions were run into a single stacking gel band on SDS-PAGE gels to remove detergents and salts. The gel band was reduced with DTT, alkylated with iodoacetic acid and digested with trypsin. Extracted peptides were re-solubilized in 0.1% aqueous formic acid and loaded onto a Thermo Acclaim Pepmap (Thermo, 75 uM ID X 2 cm C18 3 uM beads) precolumn and then onto an Acclaim Pepmap Easyspray (Thermo, 75 uM X 15 cm with 2 uM C18 beads) analytical column separation using a Dionex Ultimate 3000 uHPLC at 220 nl/min with a gradient of 2-35% organic (0.1% formic acid in acetonitrile) over 2 h. Peptides were analyzed using a Thermo Orbitrap Fusion mass spectrometer operating at 120,000 resolution (FWHM in MS1) with HCD sequencing at top speed (15,000 FWHM) of all peptides with a charge of 2+ or greater. The raw data were converted into *.mgf format (Mascot generic format) for searching using the Mascot 2.5.1 search engine (Matrix Science) against Rat protein sequences (Uniprot 2017). The database search results were loaded onto Scaffold Q+ Scaffold_4.4.8 (Proteome Sciences) for statistical treatment and data visualization.

Immunofluorescence

U2OS cells (parental and C9ORF72 KO) were transfected with LAMP1-YFP and LAMP1-RFP, respectively. LAMP1-YFP (Addgene plasmid #1816) and LAMP1-RFP (Addgene plasmid #1817) are gifts from Walther Mothes. At 24 h post transfection, both cell lines were plated on glass coverslips as a mosaic and incubated for 24 h. Cells were then fixed in 4% PFA for 10 min, and then washed 3 times. Cells were then blocked and permeabilized in blocking buffer

(TBS, 5% BSA and 0.3% Triton X-100, pH 7.4) for 1 h at room temperature. Coverslips were than incubated face down on a 50 µl drop (on paraffin film in a moist chamber) of blocking buffer containing the primary C9ORF72 antibodies diluted at 2 µg/ml and incubated overnight at 4°C. Cells were washed 3 x 10 min and incubated with corresponding Alexa Fluor 647-conjugated secondary antibodies diluted 1:1000 in blocking buffer for 2 h at room temperature. Cells were washed 3 x 10 min with blocking buffer and once with TBS. Coverslips were mounted on a microscopic slide using fluorescence mounting media (DAKO, Cat# S3023). HEK-293 (parental and C9ORF72 KO) were plated separately on coverslips and stained as mentioned above. HEK-293 cell lines were fixed in either 4% PFA for 10 min or in methanol (chilled at -20°C) for 10 min. Imaging was performed using a Leica SP8 laser scanning confocal microscope equipped with a 40x oil objective (NA = 1.30) and HyD detectors. Acquisition was performed using Leica Application Suite X software (version 3.1.5.16308) and analysis was done using Image J. All cell images represent a single focal plane. They were prepared for publication using Adobe Photoshop to adjust contrast, apply 1 pixel Gaussian blur and then assembled with Adobe Illustrator.

Immunohistochemistry with 3,3'-diaminobenzidine (DAB) staining

Formalin-fixed, paraffin-embedded brain tissue from C9-KO (n=3) and C9-wild-type (n=3) mice were sectioned at 6 µm in the sagittal plane and then mounted onto positively charged slides. Sections were deparaffinised at 60°C for 20 min on a heat block and then incubated in xylene (3 x 5 min). Subsequent rehydration was performed through graded ethanol washes and finally in water. For epitope unmasking, heat-induced epitope retrieval was carried out using TE9 buffer (10 mM Trizma base, 1 mM EDTA, 0.1% Tween 20, pH 9 at 110°C for 15 min. Endogenous peroxidases were quenched with 3% H_2O_2 in TBS for 10 min at room temperature. Slides were then blocked in 2.5% normal horse serum or 10% normal donkey serum and 0.3% Triton X-100 in TBS for 1 h at room temperature. GTX63448 and GTX632041 were diluted in DAKO antibody diluent (Agilent, Cat# S0809) at 1:5000 and then slides were incubated overnight at 4°C. Washes were then performed 3 x 10 min in TBS-0.1% Tween 20 (TBST) prior to secondary antibody incubation with ImmPRESS HRP horse anti-rabbit IgG (Vector Labs, Cat# MP-7401), ImmPRESS HRP horse anti-mouse IgG (Vector Labs, Cat# MP-7402), or HRP donkey anti-sheep IgG (1:200 in blocking buffer, Thermo Fisher Scientific, Cat# A16047) for 1 h at room temperature. Slides were then washed 3 x 20 min in TBST. DAB staining was developed under a light microscope for between 2-10 min as per the manufacturer's instructions with the ImmPACT DAB peroxidase substrate kit (Vector Labs, Cat# SK-4105). Slides were then

counterstained with Hematoxylin Solution, Gill No.1 (Sigma-Aldrich, Cat# GHS132) for 5 min at room temperature. Slides were then dehydrated with sequentially increasing graded ethanol and finally in xylene prior to coverslipping with Cytoseal 60 (Fisher Scientific, Cat# 8310-16). Micrographs were captured with an ORCA ER Hamamatsu digital camera mounted on a Leica DM6000 B upright microscope with either 10X or 40X objectives using Volocity Imaging software (version 6.3.0 PerkinElmer).

Acknowledgements

We thank Dr. Don Cleveland (UCSD) and Dr. Clothilde Lagier-Tourenne (UMass) for C9ORF72 KO mice. Proteomics analysis was performed at the Research Institute of the McGill University Health Centre Clinical Proteomics Platform. This work was supported by a grant from the Motor Neurone Disease *Association (UK), The ALS Association (USA) and ALS Canada and by an* Arthur J Hudson Team Grant from ALS Canada/Brain Canada. CL is supported by the Ronald Peter Griggs and Tim E Noël Postdoctoral Fellowship from ALS Canada. RK is supported by a studentship from the Canada First Research Excellence Fund, awarded to McGill University for Healthy Brains for Healthy Lives. JR holds the James Hunter and Family Chair in ALS Research. PSM is a James McGill Professor and a Fellow of the Royal Society of Canada.

References

Amick J, Roczniak-Ferguson A, Ferguson SM (2016) C9orf72 binds SMCR8, localizes to lysosomes, and regulates mTORC1 signaling. *Mol Biol Cell* **27**, 3040-3051.

Bradbury A and Plückthun A (2015) Reproducibility: Standardize antibodies used in research. *Nature* **518**, 27-29

DeJesus-Hernandez M, Mackenzie IR, Boeve BF, Boxer AL, Baker M, Rutherford NJ, Nicholson AM, Finch NA, Flynn H, Adamson J, Kouri N, Wojtas A, Sengdy P, Hsiung GY, Karydas A, Seeley WW, Josephs KA, Coppola G, Geschwind DH, Wszolek ZK, Feldman H, Knopman DS, Petersen RC, Miller BL, Dickson DW, Boylan KB, Graff-Radford NR, Rademakers R (2011) Expanded GGGGCC hexanucleotide repeat in noncoding region of C9ORF72 causes chromosome 9p-linked FTD and ALS. *Neuron*. **72**, 245-56

Frick P, Sellier C, Mackenzie IRA, Cheng CY, Tahraoui-Bories J, Martinat C, Pasterkamp RJ, Prudlo J, Edbauer D, Oulad-Abdelghani M, Feederle R, Charlet-Berguerand N, and Neumann M (2018) Novel antibodies reveal presynaptic localization of C9orf72 protein and reduced protein levels in C9orf72 mutation carriers. *Acta. Neuropathol. Commun*. **6**, 72.

Hornsby M, Paduch M, Miersch S, Sääf A, Matsuguchi T, Lee B, Wypisniak K, Doak A, King D, Usatyuk S, Perry K, Lu V, Thomas W, Luke J, Goodman J, Hoey RJ, Lai D, Griffin C, Li Z, Vizeacoumar FJ, Dong D, Campbell E, Anderson S, Zhong N, Gräslund S, Koide S, Moffat J, Sidhu S, Kossiakoff A, and Wells J (2015) A High Through-put Platform for Recombinant Antibodies to Folded Proteins. *Mol. Cell Proteomics* **14**, 2833-2847.

Howat, WJ, and Wilson BA (2014) Tissue fixation and the effect of molecular fixatives on downstream staining procedures. *Methods* **70**, 12-19.

Jiang J, Zhu Q, Gendron TF, Saberi S, McAlonis-Downes M, Seelman A, Stauffer JE, Jafar-Nejad P, Drenner K, Schulte D, Chun S, Sun S, Ling SC, Myers B, Engelhardt J, Katz M, Baughn M, Platoshyn O, Marsala M, Watt A, Heyser CJ, Ard MC, De Muynck L, Daughrity LM,

Kiernan MC, Vucic S, Cheah BC, Turner MR, Eisen A, Hardiman O, Burrell JR, Zoing MC (2011) Amyotrophic lateral sclerosis. *Lancet*. **377**, 942–55.

Mandegar MA, Huebsch N, Frolov EB, Shin E, Truong A, Olvera MP, Chan AH, Miyaoka Y, Holmes K, Spencer CI, Judge LM, Gordon DE, Eskildsen TV, Villalta JE, Horlbeck MA, Gilbert LA, Krogan NJ, Sheikh SP, Weissman JS, Qi LS, So PL, Conklin BR (2016) CRISPR Interference Efficiently Induces Specific and Reversible Gene Silencing in Human iPSCs. *Cell Stem Cell* **18**, 541-553.

Marcon E, Jain H, Bhattacharya A, Guo H, Phanse S, Pu S, Byram G, Collins BC, Dowdell E, Fenner M, Guo X, Hutchinson A, Kennedy JJ, Krastins B, Larsen B, Lin ZY, Lopez MF, Loppnau P, Miersch S, Nguyen T, Olsen JB, Paduch M, Ravichandran M, Seitova A, Vadali G, Vogelsang MS, Whiteaker JR, Zhong G, Zhong N, Zhao L, Aebersold R, Arrowsmith CH, Emili A, Frappier L, Gingras AC, Gstaiger M, Paulovich AG, Koide S, Kossiakoff AA, Sidhu SS, Wodak SJ, Gräslund S, Greenblatt JF, and Edwards AM (2015) Assessment of a method to characterize antibody selectivity and specificity for use in immunoprecipitation. *Nat. Methods* **12**, 725-731.

Na H, Laver JD, Jeon J, Singh F, Ancevicius K, Fan Y, Cao WX, Nie K, Yang Z, Luo H, Wang M, Rissland O, Westwood JT, Kim PM, Smibert CA, Lipshitz HD, and Sidhu SS (2016) A high-throughput pipeline for the production of synthetic antibodies for analysis of ribonucleoprotein complexes. *RNA* **22**, 636-655.

Ng AS, Rademakers R, Miller BL. (2015) Frontotemporal dementia: a bridge between dementia and neuromuscular disease. *Ann N Y Acad Sci*.**1338**, 71–93

Renton AE, Majounie E, Waite A, Simón-Sánchez J, Rollinson S, Gibbs JR, Schymick JC, Laaksovirta H, van Swieten JC, Myllykangas L, Kalimo H, Paetau A, Abramzon Y, Remes AM, Kaganovich A, Scholz SW, Duckworth J, Ding J, Harmer DW, Hernandez DG, Johnson JO, Mok K, Ryten M, Trabzuni D, Guerreiro RJ, Orrell RW, Neal J, Murray A, Pearson J, Jansen IE, Sondervan D, Seelaar H, Blake D, Young K, Halliwell N, Callister JB, Toulson G, Richardson A, Gerhard A, Snowden J, Mann D, Neary D, Nalls MA, Peuralinna T, Jansson L, Isoviita VM, Kaivorinne AL, Hölttä-Vuori M, Ikonen E, Sulkava R, Benatar M, Wuu J, Chiò A, Restagno G, Borghero G, Sabatelli M; ITALSGEN Consortium, Heckerman D, Rogaeva E, Zinman L,

Rothstein JD, Sendtner M, Drepper C, Eichler EE, Alkan C, Abdullaev Z, Pack SD, Dutra A, Pak E, Hardy J, Singleton A, Williams NM, Heutink P, Pickering-Brown S, Morris HR, Tienari PJ, Traynor BJ (2011) A hexanucleotide repeat expansion in C9ORF72 is the cause of chromosome 9p21-linked ALS-FTD. *Neuron*. **72,** 257-68

Sellier C, Campanari ML, Julie Corbier C, Gaucherot A, Kolb-Cheynel I, Oulad-Abdelghani M, Ruffenach F, Page A, Ciura S, Kabashi E, Charlet-Berguerand N (2016) Loss of C9ORF72 impairs autophagy and synergizes with polyQ Ataxin-2 to induce motor neuron dysfunction and cell death. *EMBO J*. **35**, 1276-97.

Shi Y, Lin S, Staats KA, Li Y, Chang WH, Hung ST, Hendricks E, Linares GR, Wang Y, Son EY, Wen X, Kisler K, Wilkinson B, Menendez L, Sugawara T, Woolwine P, Huang M, Cowan MJ, Ge B, Koutsodendris N, Sandor KP, Komberg J, Vangoor VR, Senthilkumar K, Hennes V, Seah C, Nelson AR, Cheng TY, Lee SJ, August PR, Chen JA, Wisniewski N, Hanson-Smith V, Belgard TG, Zhang A, Coba M, Grunseich C, Ward ME, van den Berg LH, Pasterkamp RJ, Trotti D, Zlokovic BV, and Ichida JK (2018) Haploinsufficiency leads to neurodegeneration in C9ORF72 ALS/FTD human induced motor neurons. *Nat. Med*. 24, 313-325.

Swing DA, Tessarollo L, Jung CJ, Delpoux A, Utzschneider DT, Hedrick SM, de Jong PJ, Edbauer D, Van Damme P, Petrucelli L, Shaw CE, Bennett CF, Da Cruz S, Ravits J, Rigo F, Cleveland DW, and Lagier-Tourenne C(2016) Gain of Toxicity from ALS/FTD-Linked Repeat Expansions in C9ORF72 Is Alleviated by Antisense Oligonucleotides Targeting GGGGCC-Containing RNAs. *Neuron* **90**, 535-550.

Taussig MJ, Fonseca C, and Trimmer JS. (2018) Antibody validation: a view from the mountains. *N. Biotechnol*. **25,** 1-8.

Uhlén M, Bandrowski A, Carr S, Edwards A, Ellenberg J, Lundberg E, Rimm DL, Rodriguez H, Hiltke T, Snyder M, and Yamamoto T (2016) A proposal for validation of antibodies. *Nat. Methods* **13**, 823-827.

Uhlén, M, Fagerberg, L, Hallström, BM, Lindskog, C, Oksvold, P, Mardinoglu, A, Sivertsson, Å, Kampf, C, Sjöstedt, E, Asplund, A et al. (2015) Proteomics. Tissue-based map of the human proteome. *Science* **347**, doi: 10.1126/science.1260419.

Venkataraman, A, Yang, K, Irizarry, J, Mackiewicz, M, Mita, P, Kuang, Z, Xue, L, Ghosh, D, Liu, S, Ramos, P et al. (2018) A toolbox of immunoprecipitation-grade monoclonal antibodies to human transcription factors. *Nat. Methods* **19,** doi: 10.1038/nmeth.4632.

Wang M, Herrmann CJ, Simonovic M, Szklarczyk D, and von Mering C (2015) Version 4.0 of PaxDb: Protein abundance data, integrated across model organisms, tissues, and cell-lines. *Proteomics* **15**, 3163-3168.

Zhang Y, Burberry A, Wang JY, Sandoe J, Ghosh S, Udeshi ND, Svinkina T, Mordes DA, Mok J, Charlton M, Li QZ, Carr SA, Eggan K (2018) The C9orf72-interacting protein Smcr8 is a negative regulator of autoimmunity and lysosomal exocytosis. *Genes Dev* **32**, 929-943.

Figure legends:

Figure 1: Validation of C9ORF72 antibodies by immunoblot

Cell lysates from HEK-293 parental, heterozygous (+/-) or two individual C9ORF72 KO clones (KOA, KOB) were prepared and processed for immunoblot with the indicated C9ORF72 antibodies. The arrows point to positive C9ORF72 signals. The Ponceau stained transfers associated with each blot are shown as protein loading control.

Figure 2: Testing of C9ORF72 commercial antibodies for immunoprecipitation

HEK-293 cell lysates were prepared and immunoprecipitation was performed using 1 µg of the indicated C9ORF72 antibodies pre-coupled to protein G Sepharose (prot. G) or protein A Sepharose (prot. A) as indicated. Controls included the Protein A or G alone incubated with cell lysate or protein A or G beads pre-coupled with the antibodies but incubated with lysis buffer. Samples were washed and processed for immunoblot with the indicated C9ORF72 antibodies.

Figure 3: Mass spectrometry analysis of endogenous C9ORF72 immunoprecipitation

Lysates were prepared from HEK-293 cells, parental (+/+) and KO (-/-) and immunoprecipitation was performed using C9ORF72 antibody GTX632041 pre-coupled to protein G Sepharose. The samples were prepared for immunoblot with C9ORF72 antibody PT22637. Blots were also performed for SMCR8 and WDR41. The Ponceau stained transfer associated with the blots is shown as a protein loading control. Aliquots (10%) of the cell lysates before (starting material, SM) and after incubation with the antibody-coupled beads (unbound, UB) were processed in parallel. The table shows the 3 top hits (total spectrum counts) obtained by mass spectrometry analysis of the immunoprecipitated samples.

Figure 4: Comparison of C9ORF72 protein level in cell lines and mouse tissues

(A) Lysates were prepared from mouse tissues and selective cell lines and processed for immunoblot using antibody GTX634482 with the LI-COR Odyssey Imaging System (LI-COR Biosciences) that utilizes fluorescent secondary antibodies to allow for quantitative blots (HEK = human embryonic kidney; RAW264.7 = mouse macrophage; MEF = mouse embryonic fibroblast; PC12 = rat pheochromocytoma). The total protein stained transfers are shown as loading controls. The C9ORF72 protein signal as a ratio to total protein was determined, normalized to parental HEK-293 cells (red), and presented as fold change (blue numbers). KO mouse brain (brain C9 KO) was included for specificity. **(B)** Lysates were prepared from

selective cell lines and processed for quantitative immunoblot as in **A**. (HEK = human embryonic kidney; HeLa = human cervical cancer; U2OS = human osteocarcoma; RKO = human colon carcinoma; U87/U251 = human glioblastoma; NPC = neural precursor cells; MN = human motor neurons). Quantification of C9ORF72 protein level was performed as in **A**. KO HEK-293 and KO HeLa cells were included for specificity. The total protein stained transfer on the right associated with the blot on the left is shown as a protein loading control.

Figure 5: Testing of GeneTex C9ORF72 monoclonal antibodies by immunofluorescence analysis

(A) Cell lysates of U2OS were analyzed by immunoblot. AAVS targeting gRNAs were used as a targeting control. **(B)** Mosaic strategy used to investigate antibodies specificity by immunofluorescence. **(C)** Parental and KO cells were transfected with LAMP1-YFP or LAMP1-RFP, respectively. Parental and KO cells were combined and incubated with buffer only or stained with the indicated C9ORF72 antibodies. Greyscale images of the green, red and far red channels are shown. Parental and KO cells are outlined with green and red dashed line, respectively. Representative images are shown. Bars = 40µm.

Figure 6: DAB immunohistochemistry of C9ORF72 commercial antibodies in wild-type and C9-KO mouse brain.

(A) DAB immunohistochemistry of C9ORF72 wild-type and C9ORF72 KO mouse brains in the sagittal plane using C9ORF72 antibody GTX634482. Micrographs are ordered from the rostral to caudal aspect of the mouse brain. For C9ORF72 WT arrows indicate areas of increased DAB labeling intensity and correspond to the inset regions on the right. Arrowheads indicate areas of non-specific labelling in the C9ORF72 KO mice. Scale bars = 100 μm or 25 μm for the inset images on the right for the C9ORF72 wild-type micrographs). **(B)** DAB immunohistochemistry of C9ORF72 wild-type and C9ORF72 KO mouse brains in the sagittal plane using C9ORF72 antibody GTX632041. Scale bars = 100 μm.

Supplementary Figure 1: Validation of C9ORF72 antibodies by immunoblot

Cell lysates from HEK-293 parental, heterozygous (+/-) or two individual C9ORF72 KO clones (KOA, KOB) were prepared and processed for immunoblot with the indicated C9ORF72 antibodies. The arrows point to positive C9ORF72 signals.

Supplementary Figure 2: Testing of C9ORF72 antibodies by immunofluorescence analysis in HEK-293 cells fixed with PFA

HEK-293 parental and KO cells were fixed with PFA, permeabilized and incubated with the indicated C9ORF72 antibodies. Representative images are shown. Bars = 16µm.

Supplementary Figure 3: Testing of C9ORF72 antibodies by immunofluorescence analysis in HEK-293 cells fixed with -20°C methanol.

HEK-293 parental and KO cells were fixed with -20°C methanol, permeabilized and incubated with the indicated C9ORF72 antibodies. Representative images are shown. Bars = 16µm.

Supplementary Figure 4: Testing of 12 C9ORF72 antibodies by immunofluorescence analysis

Parental and KO cells were transfected with LAMP1-YFP or LAMP1-RFP, respectively. Parental and KO cells were combined and incubated with buffer only or stained with the indicated C9ORF72 antibodies. Greyscale images of the far-red channel is shown. Parental and KO cells are outlined with green and red dashed line, respectively. Representative images are shown. Bars = 40µm.

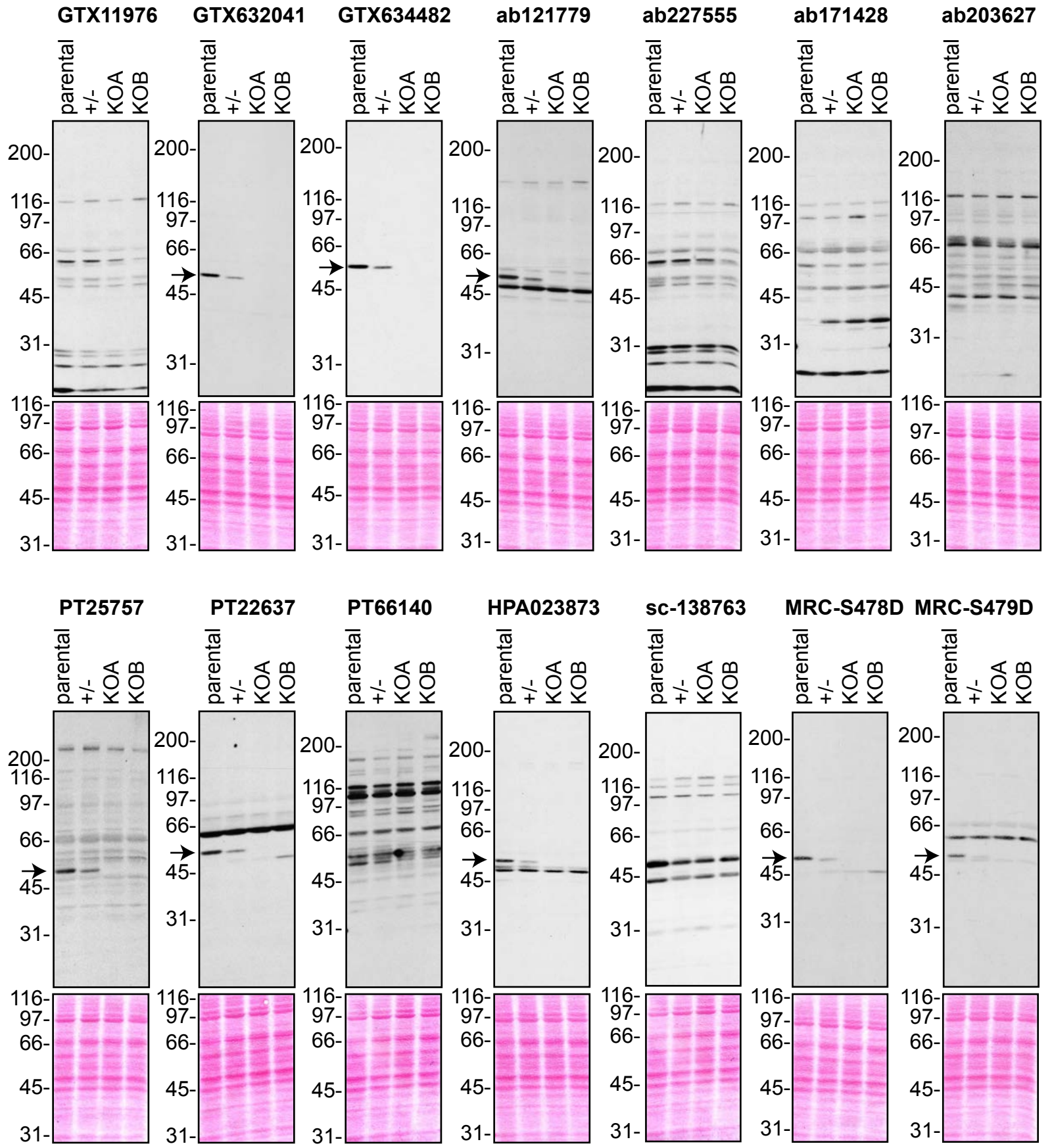

Laflamme *et al*., Figure 1

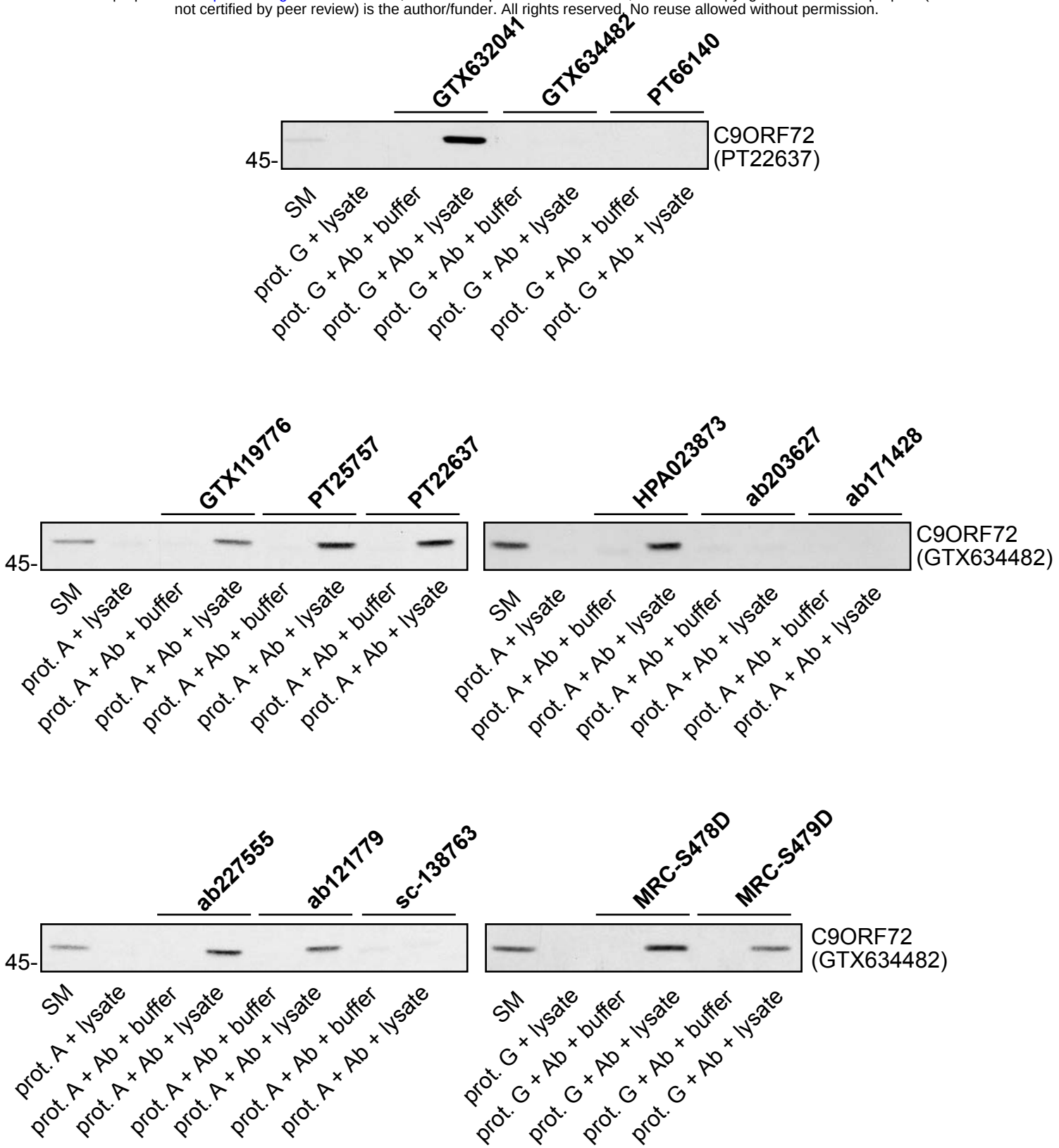

Laflamme *et al*., Figure 2

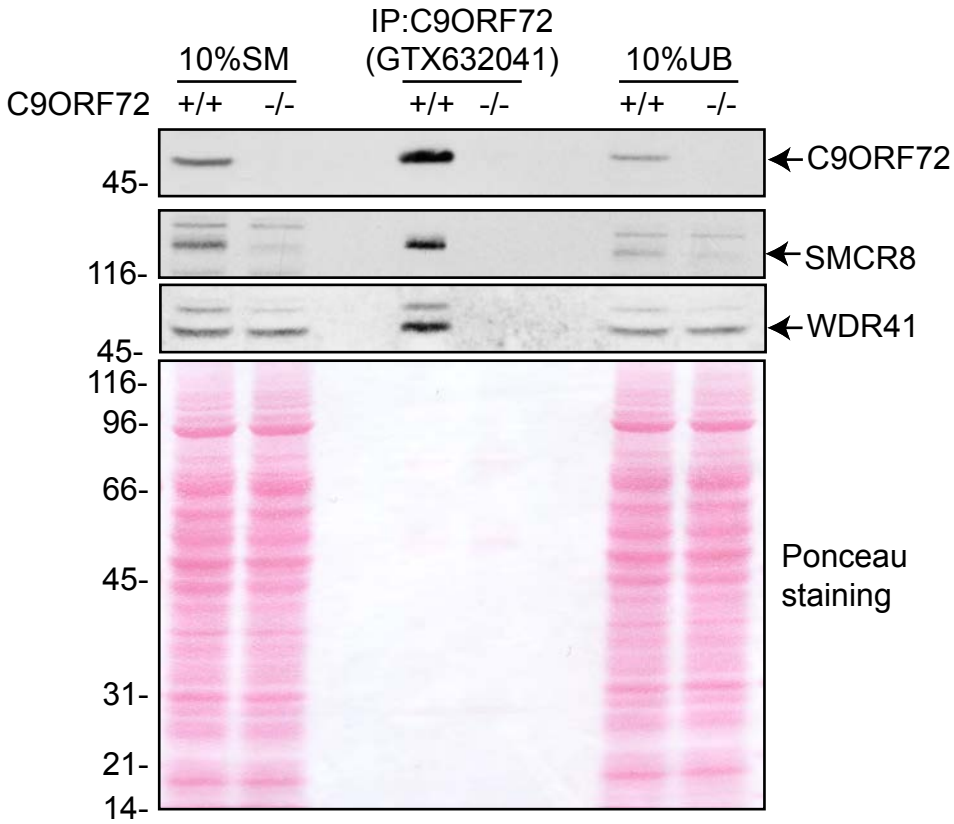

#	Identified proteins	Percent coverage	Total spectrum count
1	SMCR8	45%	51
2	WDR41	46%	23
3	C9ORF72	19%	13

Laflamme *et al*., Figure 3

A

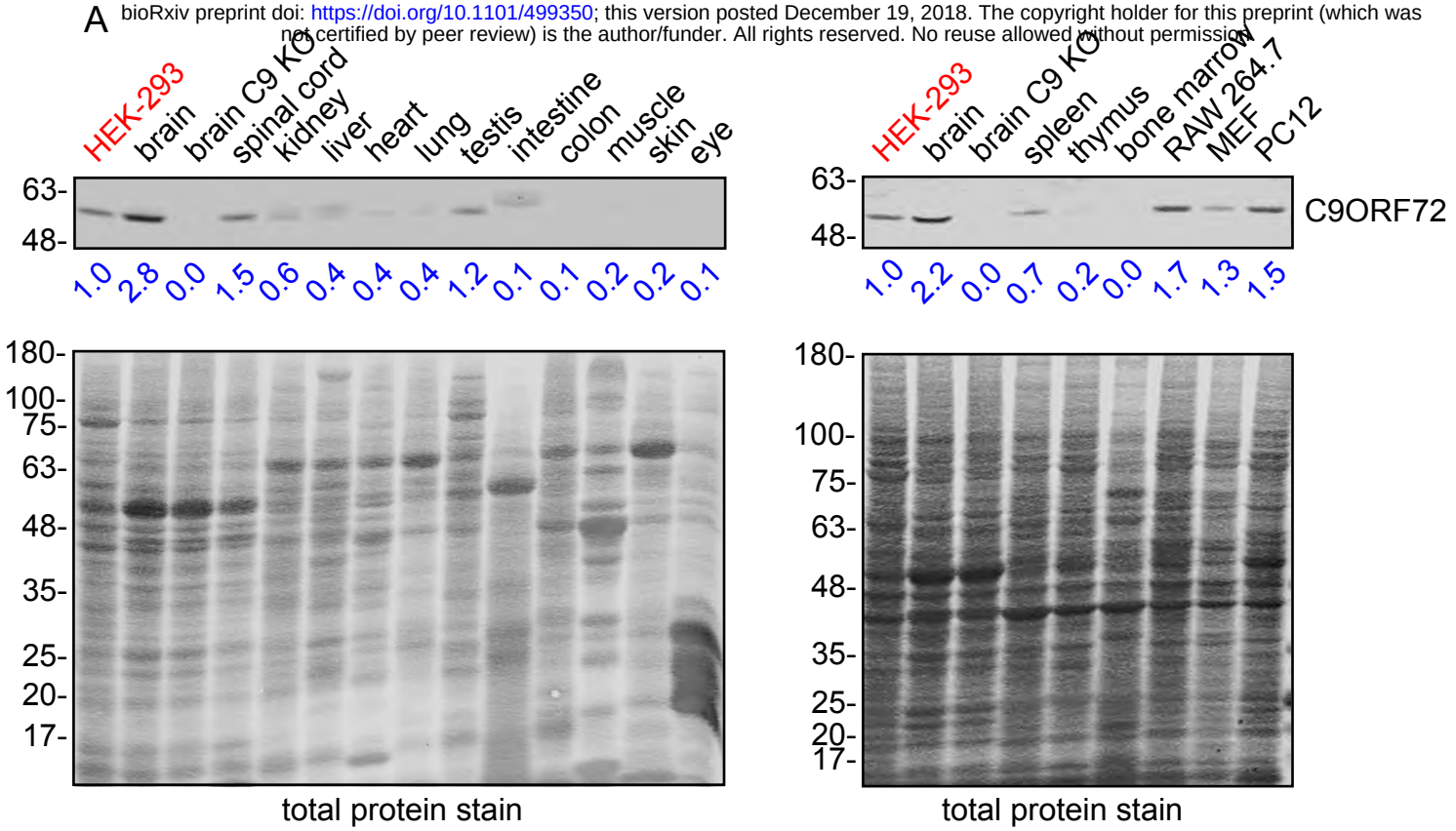

B

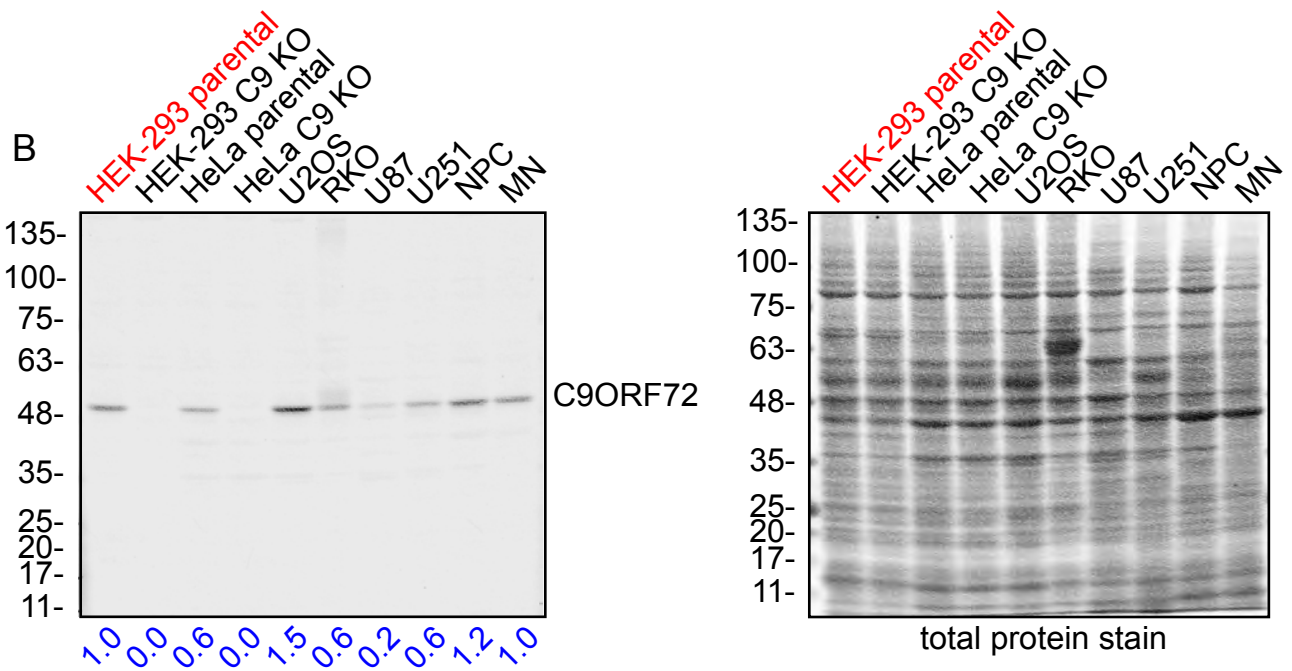

Laflamme *et al*., Figure 4

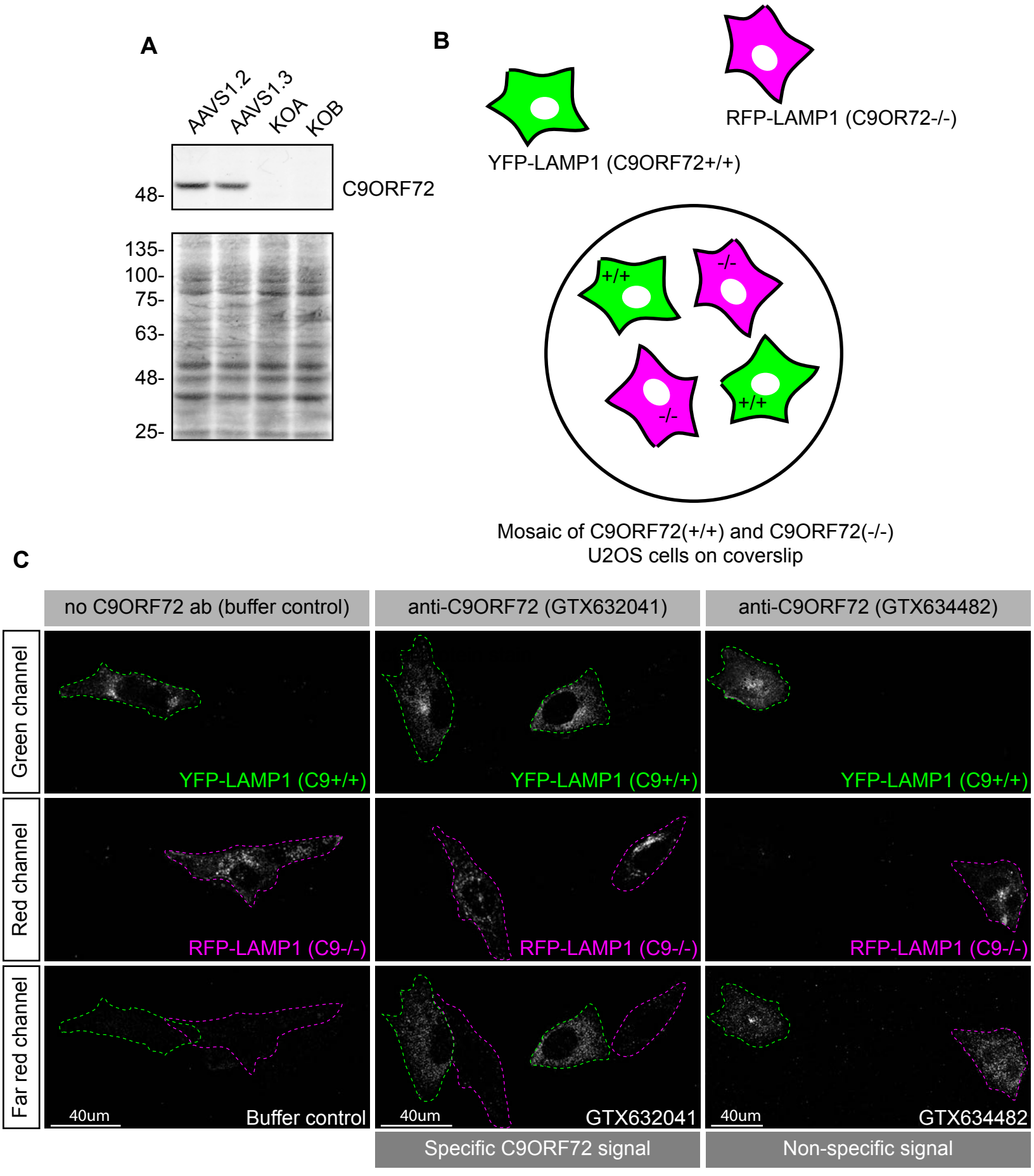

Laflamme *et al.*, Figure 5

GTX634482 **GTX632041**

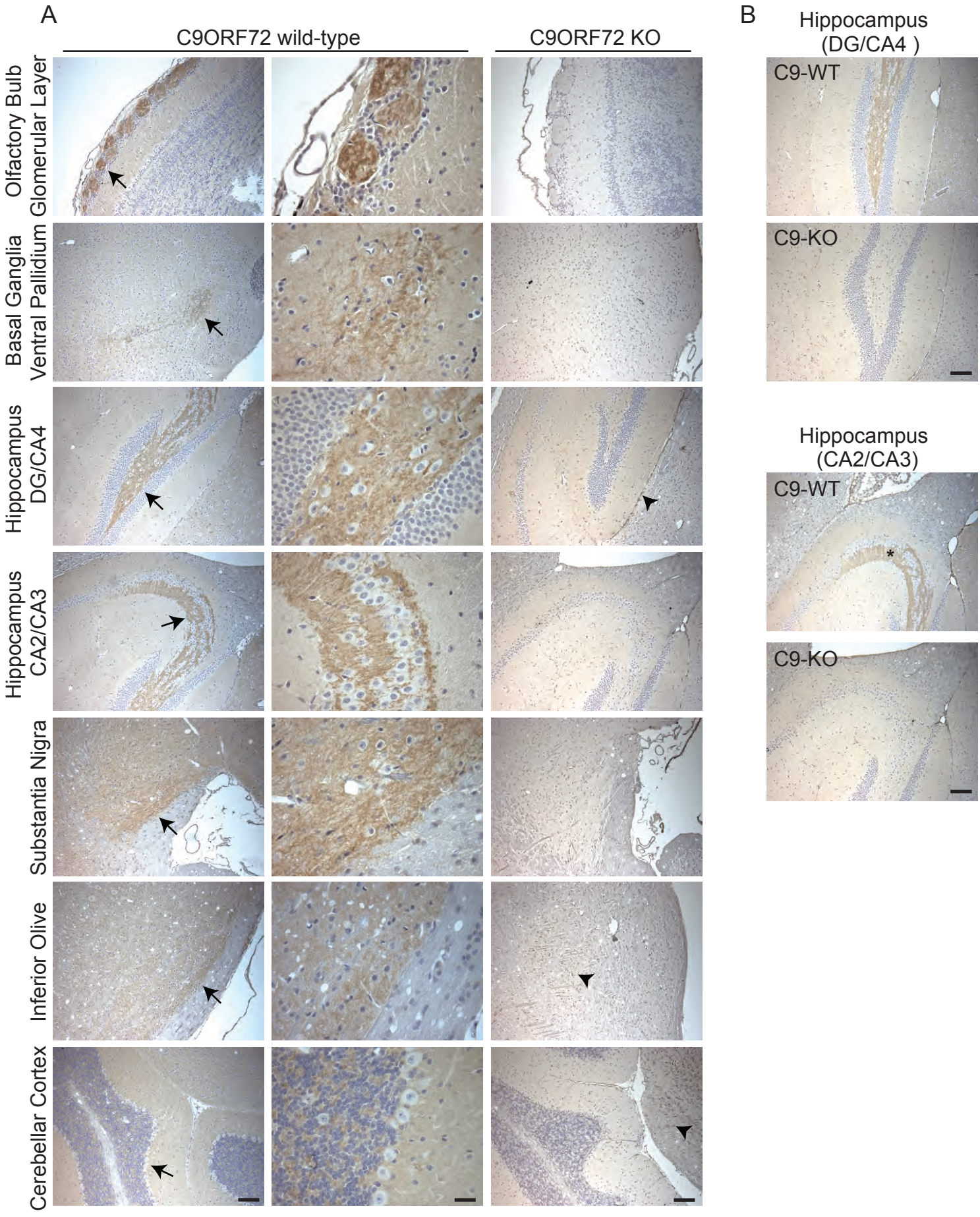

Laflamme *et al*., Figure 6

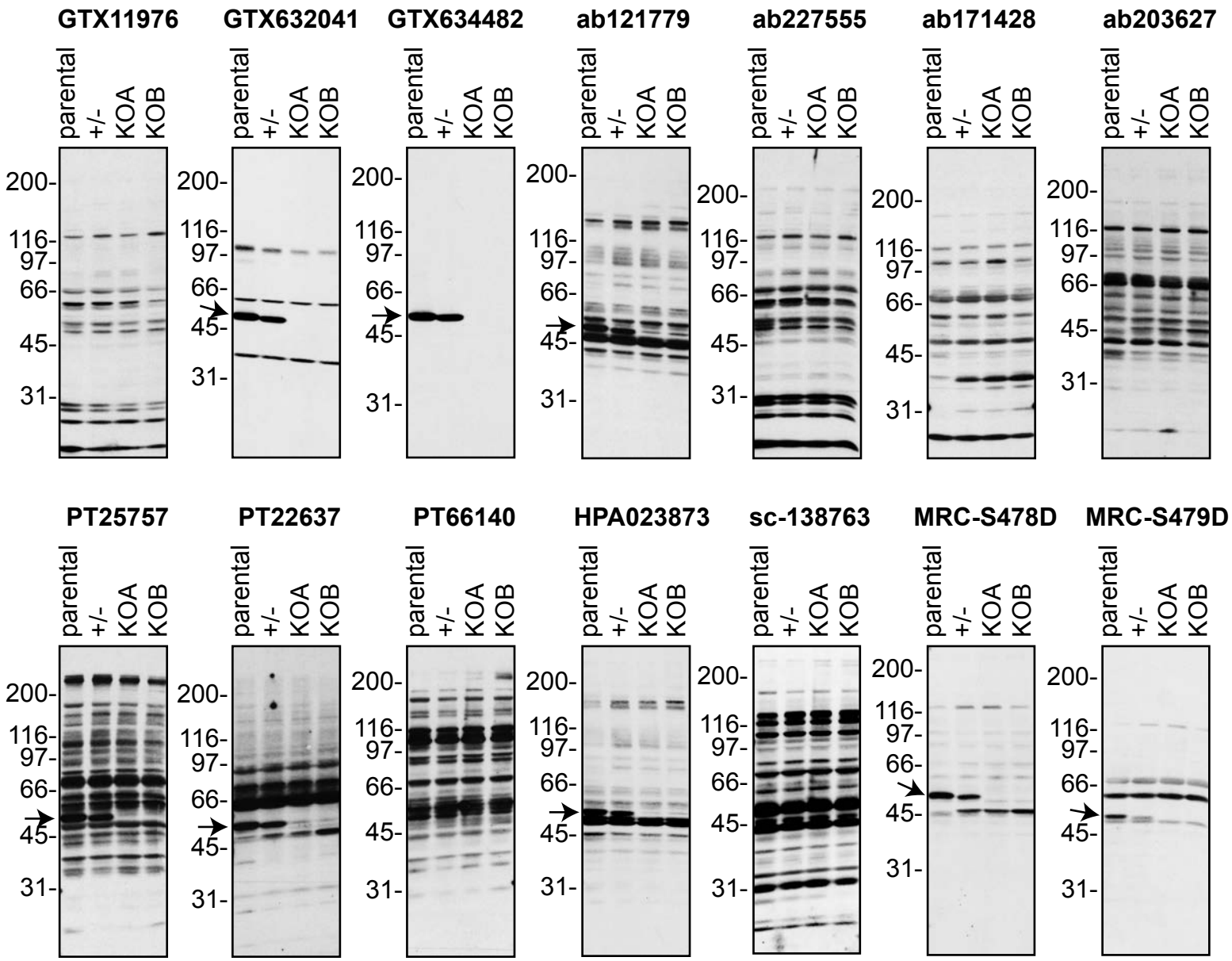

Laflamme *et al*., Supplementary Figure 1

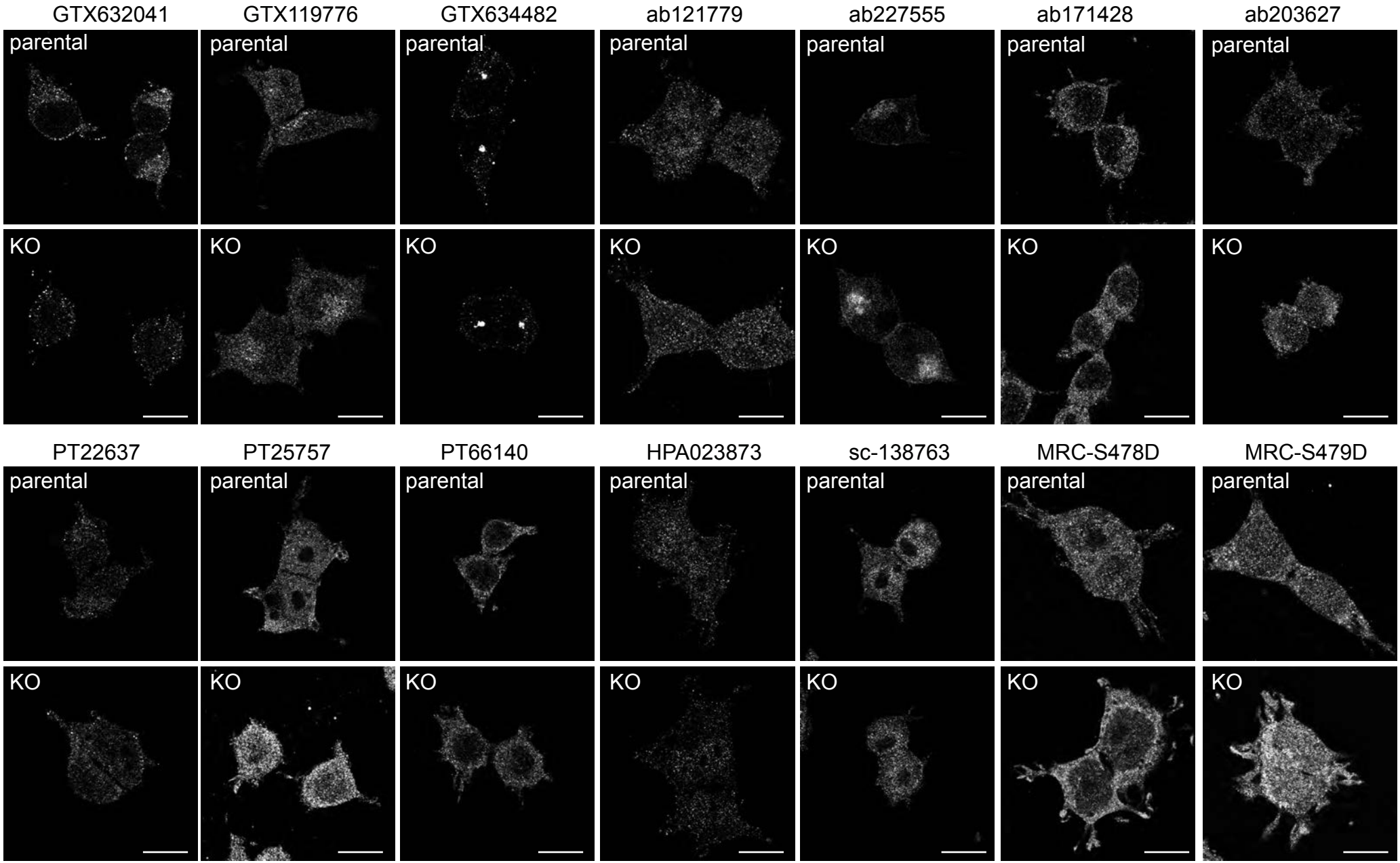

Laflamme *et al*., Supplemental Figure 2

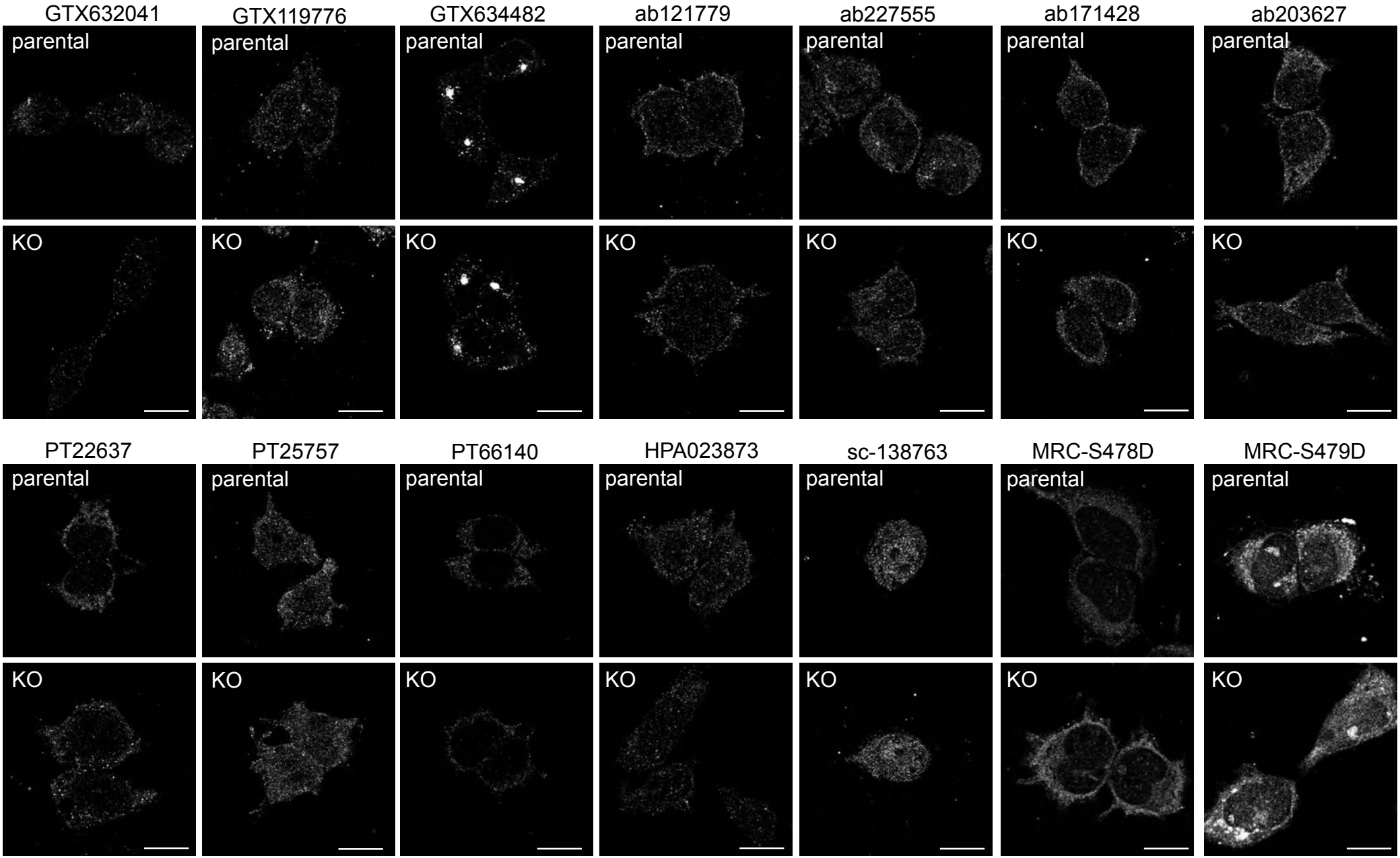

Laflamme *et al*., Supplemental Figure 3

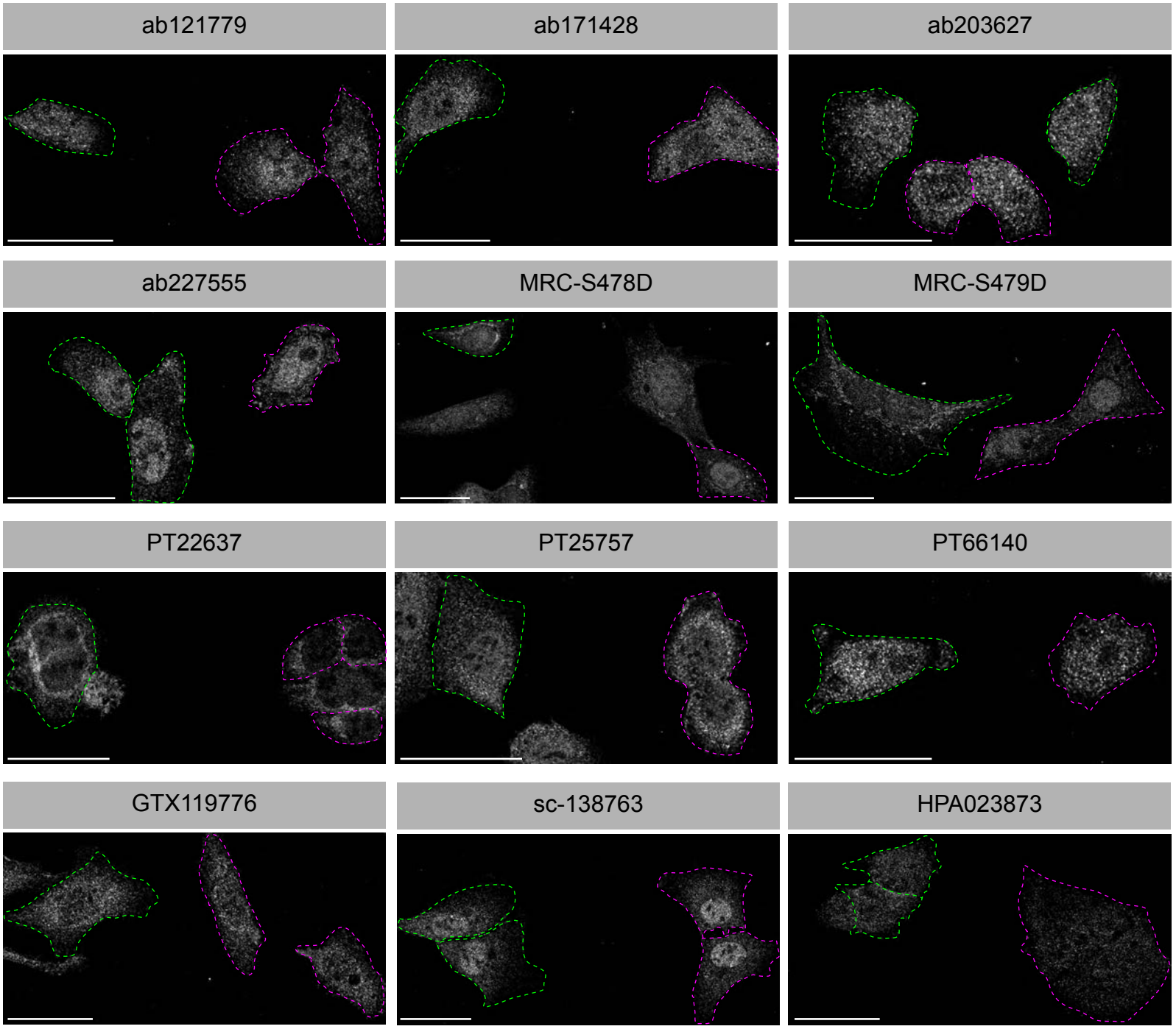

Laflamme *et al*., Supplemental Figure 4